FEBS Letters

FEBS PRESS science publishing by scientists

Telencephalon-specific *Alkbh1* conditional knockout mice display hippocampal atrophy and impaired learning

Layla Kawarada[1,2], Masahiro Fukaya[3], Ryo Saito[1], Hidetoshi Kassai[1], Hiroyuki Sakagami[3] and Atsu Aiba[1,2]

1 Laboratory of Animal Resources, Center for Disease Biology and Integrative Medicine, Graduate School of Medicine, The University of Tokyo, Japan

2 Department of Biological Sciences, School of Science, The University of Tokyo, Japan

3 Department of Anatomy, Kitasato University School of Medicine, Sagamihara, Japan

Correspondence

A. Aiba, Laboratory of Animal Resources, Center for Disease Biology and Integrative Medicine, Graduate School of Medicine, The University of Tokyo, 7-3-1 Hongo, Bunkyo-ku, Tokyo 113-0033, Japan

Tel: +81 3 5841 3638

E-mail: aiba@m.u-tokyo.ac.jp

(Received 25 February 2021, revised 14 April 2021, accepted 16 April 2021, available online 19 May 2021)

doi:10.1002/1873-3468.14098

Edited by Ned Mantei

AlkB homolog 1 (ALKBH1) is responsible for the biogenesis of 5-formylcytidine (f^5C) on mitochondrial $tRNA^{Met}$ and essential for mitochondrial protein synthesis. The brain, especially the hippocampus, is highly susceptible to mitochondrial dysfunction; hence, the maintenance of mitochondrial activity is strongly required to prevent disorders associated with hippocampal malfunction. To study the role of ALKBH1 in the hippocampus, we generated dorsal telencephalon-specific *Alkbh1* conditional knockout (cKO) mice in inbred C57BL/6 background. These mice showed reduced activity of the respiratory chain complex, hippocampal atrophy, and CA1 pyramidal neuron abnormalities. Furthermore, performances in the fear-conditioning and Morris water maze tests in cKO mice indicated that the hippocampal abnormalities led to impaired hippocampus-dependent learning. These findings indicate critical roles of ALKBH1 in the hippocampus.

Keywords: Alkbh1; hippocampus; knockout mice; learning and memory; mitochondria

Mitochondria are essential intracellular organelles that produce approximately 90% of whole-body energy expenditure. Some components of the respiratory chain complex are synthesized in the mitochondrial own translation system, and mitochondrial genetic code has an anomalous codon correspondence that differs from that of the cytoplasm [1]. The AUA codon, which specifies isoleucine in the universal code, is converted to methionine. To decode the AUA codon as methionine, mt-$tRNA^{Met}$ contains a unique modification, 5-formylcytidine (f^5C), at the wobble position (position 34) [2]. An *in vitro* mitochondrial translation system demonstrated that f^5C enables mt-$tRNA^{Met}$ to decode both the AUA and AUG codons [3]. Previously, we and others identified Fe^{2+}/2-oxoglutarate (2-OG)-dependent dioxygenase AlkB homolog 1 (ALKBH1) as one of the enzymes responsible for f^5C formation [4–6]. Cultured human cells lacking ALKBH1 showed a marked reduction in mitochondrial protein synthesis and respiratory activity [5]. In addition to f^5C formation in mt-$tRNA^{Met}$, ALKBH1 is also reportedly involved in cellular functions in the nucleus and cytoplasm, including the formation of 5-hydroxymethyl-2′-*O*-methylcytidine (hm^5Cm) and 5-formyl-2′-*O*-methylcytidine (f^5Cm) in cytoplasmic $tRNA^{Leu}$ [5], demethylation of N^1-methyladenosine (m^1A) in cytoplasmic and mitochondrial tRNAs [5,7,8], N^6-methyladenosine (m^6dA) in

Abbreviations

2-OG, 2-oxoglutarate; ALKBH1, AlkB homolog 1; cKO, conditional knockout; f^5C, 5-formylcytidine; mt, mitochondrial; NSUN3, NOL1/NOP2/Sun domain-containing protein 3; ROS, reactive oxygen species; sgRNA, single-guide RNA.

genomic DNA [9,10], and N^6-methyladenosine (m^6A) in mRNA [11]. It has also been suggested that ALKBH1 may exert its function in a cell type-specific manner. Liu *et al.* [7] demonstrated the ability of ALKBH1 to demethylate m^1A in cytoplasmic tRNAs in HeLa and mouse embryonic fibroblast (MEF) cells, whereas no activity was observed in human glioblastoma cells [10].

Mitochondrial dysfunction causes severe damage to various organs through reduced ATP production, reactive oxygen species (ROS) production, and accelerated cell death. The brain is susceptible to mitochondrial dysfunction owing to its high energy demands. The hippocampus is one of the most vulnerable regions in the brain to oxidative stress caused by mitochondrial dysfunction due to aging or ischemia. The vulnerability could be attributed to low expression of superoxide dismutase (SOD), which removes ROS, and high activity of mitochondrial permeability transition pore (mPTP), which releases the pro-apoptotic factor cytochrome c, in the hippocampus [12,13]. Indeed, Alzheimer's disease patients, in whom hippocampal atrophy and loss of hippocampal neurons are observed, frequently exhibit mitochondrial abnormalities [14]. To elucidate the physiological role of ALKBH1, a key factor in the maintenance of mitochondrial function, in the hippocampus, we generated dorsal telencephalon-specific *Alkbh1* conditional knockout (cKO) mice using *Emx1-Cre* mice.

The whole-body *Alkbh1* KO mice we constructed showed decreased survival and body weight, suggesting that ALKBH1 is indispensable for proper perinatal development. Furthermore, dorsal telencephalon-specific *Alkbh1* cKO mice displayed age-related hippocampal atrophy and CA1 pyramidal neuron abnormalities. Behavioral tests, including fear-conditioning and Morris water maze tests, were conducted and showed hippocampus-dependent learning and memory deficits in the *Alkbh1* cKO mice.

Materials and methods

Animals

Animal experiments were approved by the Institutional Animal Care and Use Committee of the University of Tokyo (Permission No. M-P16-048) and conducted according to the University of Tokyo guidelines. All staff involved in the animal experiments attended designated training on animal experiments and obtained a certificate of completion at the University of Tokyo. The mice were maintained on a 12:12-h light–dark cycle in a room with controlled humidity and temperature, with food and water available *ad libitum*. Their health and behavior were monitored by trained experimenters and veterinarians as necessary at daily frequencies based on food and water intake, and mouse activity.

Appropriate measures were adopted to reduce or eliminate the suffering and distress inflicted on the animals as much as possible. Mice showing severe pain and/or distress, including reduced activity, hunched appearance, ruffled hair coat, respiratory distress, and weight loss, were euthanized by CO_2 asphyxiation. Experiments using the whole-body KO mice were carried out by 8 weeks of age. Conditional KO mice that did not show apparent health problems were used by 1 year of age. The number of mice used in the experiment was the minimum necessary to obtain statistically significant data.

Generation of the whole-body KO and dorsal telencephalon-specific *Alkbh1* cKO mice

To generate *Alkbh1*-flox (*Alkbh1*$^{flox/flox}$) mice, we used CRISPR/Cas9 system by electroporating two single-guide RNAs (sgRNAs) flanking exon 3 of the *Alkbh1* gene and *loxP* sites containing single-stranded oligonucleotides (ssODNs) together with the Cas9 protein into C57BL/6N mouse zygotes, as described previously [15]. In addition to *Alkbh1*-flox mice by homologous recombination, we obtained *Alkbh1* heterozygous null mutant (*Alkbh1*$^{+/-}$) mice by deleting the entire exon 3 *via* nonhomologous end-joining. The whole-body KO (*Alkbh1*$^{-/-}$) mice were generated by crossing the *Alkbh1*$^{+/-}$ pairs. To produce dorsal telencephalon-specific *Alkbh1* cKO (*Alkbh1*$^{flox/-}$;*Emx1*$^{Cre/+}$) mice, we first mated *Alkbh1*$^{+/-}$ mice with *Emx1*$^{Cre/+}$ mice [16] to obtain *Alkbh1*$^{+/-}$;*Emx1*$^{Cre/+}$ mice. The *Alkbh1*$^{+/-}$;*Emx1*$^{Cre/+}$ mice were then crossed with *Alkbh1*$^{flox/flox}$ mice to generate *Alkbh1*$^{flox/-}$;*Emx1*$^{Cre/+}$ mice. The mice were genotyped by polymerase chain reaction (PCR) of genomic DNA extracted from their tails.

The sequences for the sgRNAs, ssODNs, and PCR primers are as follows:

5′-sgRNA: GCGAACCTTCAGTTCTGAA.

3′-sgRNA: TCAATTGGGTACCTAGGCAT.

5′-ssODN: C*T*CTGCCTCCCAAGTGCTGGGATTAAAGGCGTGCGCCACCATGCCCGGCGATAACTTCGTATAGCATACATTATACGAAGTTATGAATTCAACCTTCAGTTCTGAAGTTGCTTTAGGATAGCACTGTTGACAGCTAAC*C*T

3′-ssODN: C*T*AATCACTATTAAAGAGTGTCCATATCCTAAAGTTTTGTGTCTCCAATGGAATTCATAACTTCGTATAATGTATGCTATACGAAGTTATCCTAGGTACCCAATTGATTTCTCCAATGAGTATTTGTGGAATGAATGC*T*G

*Phosphorothioate modification.

Alkbh1 flox Fw: 5′-ATGGGTCGGTTGTTGCTCAT-3′

Alkbh1 flox Rv: 5′-CATTCACCCTGTTTGGAAGAA-3′
Alkbh1 del Fw: 5′-TGCAAAAGTGACTTGGGGGA-3′
Alkbh1 del Rv: 5′-GTGACTGCCAGGAAGCATCT-3′

Immunoblot analysis

The cerebral cortex and hippocampus were isolated and lysed in RIPA buffer consisting of 50 mM Tris/HCl (pH 8.0), 150 mM NaCl, 1% Triton X-100, 0.5% sodium deoxycholate, 0.1% sodium dodecyl sulfate, and 1× complete mini protease inhibitor cocktail tablet (Roche, Basel, Switzerland). ALKBH1 expression was detected by immunoblotting using an anti-ALKBH1 antibody (1:1000, ab128895, Abcam, Cambridge, UK) and horseradish peroxidase-conjugated anti-rabbit immunoglobulin G (1:10000 Jackson ImmunoResearch, West Grove, PA, USA). The signals were visualized using ECL Plus detection reagents (GE Healthcare Bio-Sciences Corp, Piscataway, NJ, USA).

Measurement of respiratory chain complex I activity

To fractionate mitochondria, the hippocampi of control and *Alkbh1* cKO mice were homogenized using a Teflon homogenizer in 3-(N-morpholino) propanesulfonic acid (MOPS) buffer consisting of 250 mM sucrose, 10 mM MOPS (pH 7.2), and 1× complete mini protease inhibitor cocktail tablet (Roche). The homogenate was centrifuged at 800 × g for 5 min at 4 °C. The supernatant was further centrifuged at 8000 × g for 20 min at 4 °C. The mitochondrial pellet was collected and resuspended in MOPS buffer. The respiratory chain complex I activity was evaluated as previously described [17].

Behavioral tests

Behavioral tests were performed as previously described [18]. All the mice were male littermates. The experimenter was blinded to the genotypes during the experiments. Mice were acclimatized to the experimental environment by leaving them in the test room for at least 1 h before testing.

Fear-conditioning test

Fear-conditioning tests were performed using ImageJ FZ1 (O'Hara & Co., Ltd., Tokyo, Japan). On day 1 (conditioning session), the mouse was placed in a cubic chamber (10 cm × 10 cm × 10 cm) with a grid metal floor connected to an electric shock generator. Mouse movements were recorded using a camera mounted above the chamber. After the mouse had been acclimatized to the chamber environment for the first 3 min, the mouse was administered a combined tone (65 dB white noise) and footshock stimuli (30 s of tone, 2 s of 0.8 mA footshock at the end of the tone) twice at 1-min intervals for conditioning. The mouse was left in the chamber for 1 min after the second footshock and then returned to its home cage. On day 8 (context session), the mouse was placed in the same chamber in which the conditioning had been performed, and freezing was measured for 6 min without tone or footshock. On day 9 (cued session), the mouse was placed in a novel chamber different from the conditioning chamber. Freezing was measured for 3 min without stimulation (pretone), followed by the same tone as the conditioning for 3 min (tone). Freezing was defined as a stay at rest for > 2 s.

Morris water maze test

The Morris water maze consists of a pool (120 cm diameter, 30 cm height) filled with water to a depth of 24 cm and a platform (10 cm diameter, 23 cm height). The platform was placed in the target quadrant of the pool and submerged in water that was cloudy to match the poster color so that it was not visible to the mice. Four different visual cues were affixed to a height of 50 cm on the blackout curtain surrounding the pool. The tests were conducted under 15 lux illumination. On days 1–5, the mice were subjected to a spatial learning session, and on day 6, they were subjected to a probe test. Each spatial learning session consisted of four trials. In each trial, the mice were released and allowed to swim for up to 1 min to explore the platform. The latency to reach the platform was then measured. Mice that did not reach the platform were guided to the platform by the experimenter and made to memorize the location of the platform. In the probe test on day 6, the platform was removed, the mice were left to swim, and the time spent in each quadrant was measured.

Histological analysis

To fix the adult mouse brain, the mice were transcardially perfused with 4% paraformaldehyde in 0.1 M phosphate buffer (pH 7.4). Extracted brains were postfixed overnight, immersed in 30% sucrose solution in phosphate-buffered saline, and then sectioned into 30-µm-thick parasagittal slices using a freezing microtome (FX-801, COPER, Kanagawa, Japan). To analyze the P0 mouse brain, pups were retrieved from pregnant mice by cesarean section and the brains were immediately removed and kept in 4% paraformaldehyde in 0.1 M phosphate buffer for 3 h. Slices were prepared using a cryostat (CM1850, Leica Microsystems, Nussloch, Germany) with a thickness of 20 µm. For quantification of the hippocampal area, Nissl staining was performed by dipping the slices in 0.1% cresyl violet. The Nissl-stained sections were photographed at 10× magnification in a bright field by fluorescence microscopy (BZ-800

Keyence, Osaka, Japan). The hippocampal areas of the images were measured using ImageJ software by delineating with reference to the Allen Mouse Brain Atlas (https://mouse.brain-map.org/).

Electron microscopy

Three 27 week-old male mice of each genotype were perfused transcardially with 2% paraformaldehyde/2.5% glutaraldehyde in 0.1 M phosphate buffer for electron microscopic analyses. Parasagittal brain sections (200 µm thick) were further postfixed with 1% osmium tetroxide for 1 h, stained with 2% uranyl acetate for 1 h, dehydrated with gradient alcohol, and embedded in Epon 812 resin. Ultrathin sections (75 nm thick) of the hippocampus were cut using an ultramicrotome (Ultracut; Leica, Nussloch, Germany). Electron microscopy images were obtained using an electron microscope (H7650; Hitachi, Tokyo, Japan). The mitochondrial width of pyramidal cells in the hippocampal CA1 region was measured using ImageJ software (NIH, Bethesda, MD, USA).

Results

Generation of the whole-body *Alkbh1* KO mice

To generate *Alkbh1* KO mice, we used the CRISPR/Cas9-mediated exon skipping approach in inbred C57BL/6N zygotes. We expected complete disruption of *Alkbh1* function by introducing frameshift mutations into exon 4, because exons 4–6 encode functional domains [19]. Therefore, we focused on exon 3 as an exon-skip target and designed two sgRNAs in the introns on both sides of exon 3 (Fig. 1A). We then electroporated two sgRNAs into the cytoplasm of C57BL/6N zygotes and subsequently obtained mutant mice carrying the desired deletion of exon 3 (Fig. 1A,B). This deletion resulted in a frameshift mutation with a stop codon in exon 4 (Fig. 1A). The lack of exon 3 was confirmed by PCR of genomic DNA and sequencing of the region flanking exon 3 (Fig. 1B).

Decreased survival rate of the whole-body *Alkbh1* KO mice

In a previous study, a reduced survival rate and non-Mendelian distribution were observed in the *Alkbh1*$^{-/-}$ offspring obtained from heterozygous crosses (*Alkbh1*$^{+/-}$ × *Alkbh1*$^{+/-}$) [20]. The ratio of survival of *Alkbh1*$^{-/-}$ pups was much lower than the theoretical value (Fig. 1C), consistent with the previous report [20]. Furthermore, the body weight at 3 weeks of age was significantly lower in *Alkbh1*$^{-/-}$ females (Fig. 1D). However, the difference in the body weight between *Alkbh1*$^{-/-}$ and *Alkbh1*$^{+/+}$ males was not statistically significant, likely because of the small number of surviving *Alkbh1*$^{-/-}$ mice (Fig. 1D).

Generation of mice with dorsal telencephalon-specific conditional knockout for *Alkbh1*

To analyze the physiological role of *Alkbh1* in the central nervous system, mainly focusing on the hippocampus, we generated cKO mice lacking *Alkbh1* in the excitatory glutamatergic neurons of the dorsal telencephalon (*Alkbh1*$^{flox/-}$;*Emx1*$^{Cre/+}$). We first generated mutant mice with *loxP* sequences inserted into introns flanking exon 3 of *Alkbh1* (*Alkbh1*-flox mice) by CRISPR/Cas9-mediated knock-in using ssODNs as templates for homology-directed repair (Fig. 2A). Next, to obtain *Alkbh1*$^{flox/-}$;*Emx1*$^{Cre/+}$ mice, we crossed *Alkbh1*-flox and *Emx1*$^{Cre/+}$ mice. *Emx1*$^{Cre/+}$ mice carrying the *cre* gene under the control of *Emx1* promoter express Cre recombinase exclusively in the dorsal telencephalon from embryonic day (E) 10.5 to adulthood [16,21]. In this study, we used *Alkbh1*$^{flox/-}$; *Emx1*$^{Cre/+}$ mice as dorsal telencephalon-specific cKO mice, and *Alkbh1*$^{flox/+}$; *Emx1*$^{+/+}$ mice as control. Immunoblot analysis showed the significant reduction in ALKBH1 protein expression in the hippocampus and cerebral cortex of the *Alkbh1* cKO mice (Fig. 2B). ALKBH1 bands in the cKO lanes probably originated from the glial cells and/or inhibitory neurons that did not express Cre. The *Alkbh1* cKO mice showed normal body weights (Fig. 2C). Since the mitochondrial function was impaired in cultured human cells lacking ALKBH1 [5], we compared the respiratory complex I activity of mitochondria between *Alkbh1* cKO and control hippocampi. We found the significantly reduced complex I activity in the hippocampi of *Alkbh1* cKO mice (Fig. 2D).

Alkbh1 deletion induced hippocampal atrophy and abnormal CA1 pyramidal neurons

Previous studies have reported that ALKBH1 is highly expressed during the embryonic stage and is important for neural differentiation [22]. *Alkbh1*$^{+/-}$ and *Alkbh1*$^{-/-}$ mice also showed disrupted neural tube closure and exencephaly [20,22]. However, we observed no obvious abnormalities in neural tube closure in *Alkbh1*$^{-/-}$ mice at E10.5 or E14.5 (data not shown).

Mitochondrial dysfunction causes reduced ATP production, ROS-mediated oxidative stress, and activation of the mPTP, which consequently lead to cell death. In the central nervous system, the hippocampal CA1

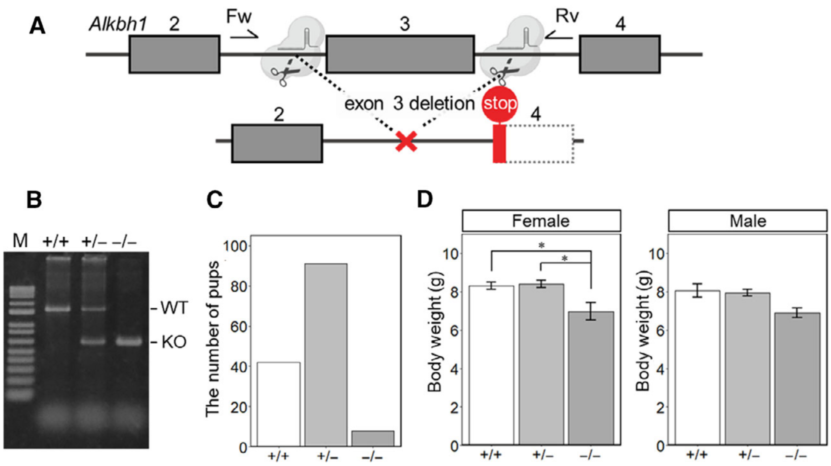

Fig. 1. The whole-body *Alkbh1* KO mice showed decreased survival rates and reduced body weight. (A) Schematic diagrams of strategies for deletion of exon 3 of the mouse *Alkbh1* gene by the CRISPR/Cas9 system. The filled boxes represent coding exons. Deletion of exon 3 leads to premature termination of translation in exon 4 as indicated. Two PCR primers for genotyping (Fw and Rv) and two target sites for sgRNA are indicated. (B) Genotyping PCR analysis of a wild-type mouse (+/+), a heterozygote (+/–), and a homozygote (–/–). Wild-type (WT) and knockout (KO) bands are corresponding to 1599-bp and 631-bp PCR products, respectively. M, DNA size marker. (C) The number of 3-week-old pups obtained by crossing between *Alkbh1*$^{+/-}$ mice. (D) The body weight of female (left) and male (right) mice at 3 weeks of age (female: +/+, n = 23; +/–, n = 43; –/–, n = 5. male: +/+, n = 19; +/–, n = 48; –/–, n = 3). Values are means ± SEM. **p* < 0.05, Student's *t*-test.

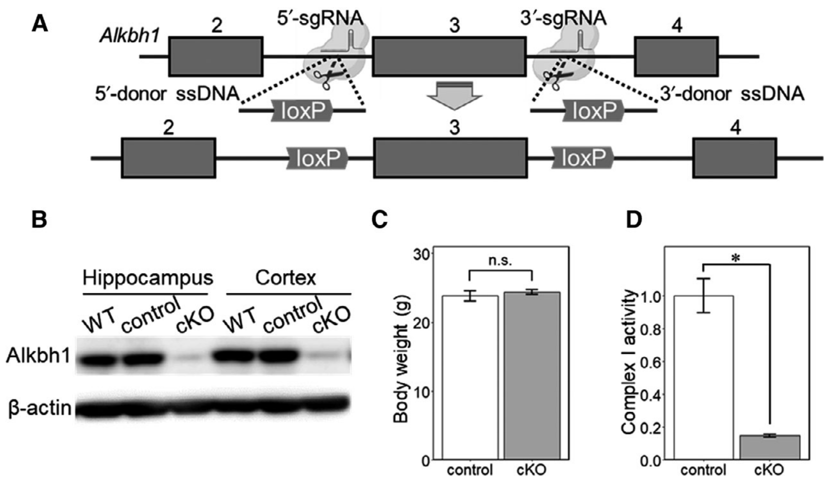

Fig. 2. Generation of dorsal telencephalon-specific *Alkbh1* cKO mice. (A) Schematic diagrams of strategies for inserting *loxP* sequences into target regions to generate *Alkbh1*-flox mice. (B) Immunoblot analysis of ALKBH1 protein expression in the hippocampus and the cerebral cortex of *Alkbh1*$^{+/+}$;*Emx1*$^{+/+}$ (WT), *Alkbh1*$^{flox/+}$;*Emx1*$^{+/+}$ (control) and *Alkbh1*$^{flox/-}$;*Emx1*$^{Cre/+}$ (cKO) mice at 6–7 weeks of age. β-Actin was used as loading controls. (C) The body weight of control and *Alkbh1* cKO mice at 9 weeks of age. (D) The activity of respiratory chain complex I in control and *Alkbh1* cKO mice. Activities of the respiratory chain complex I of mitochondria fractionated from the hippocampus of 46-week-old mice. The activity is normalized against that of control mice. n = 2 for each genotype. Values are means ± SEM. **p* < 0.05, Student's *t*-test.

region is especially vulnerable to mitochondrial dysfunction and is highly susceptible to oxidative stress caused by aging or brain ischemia [13,23]. Since mitochondrial respiratory chain complex function was markedly decreased in the hippocampus of *Alkbh1* cKO mice (Fig. 2D), we hypothesized that the loss of *Alkbh1* in the dorsal telencephalon may affect hippocampal neuron survival. Although we found no apparent abnormality in the Nissl-stained sagittal sections of the *Alkbh1* cKO brains at P0, the hippocampal area of *Alkbh1* cKO mice was significantly smaller than that of the control at 12 weeks of age (Figs 3A,

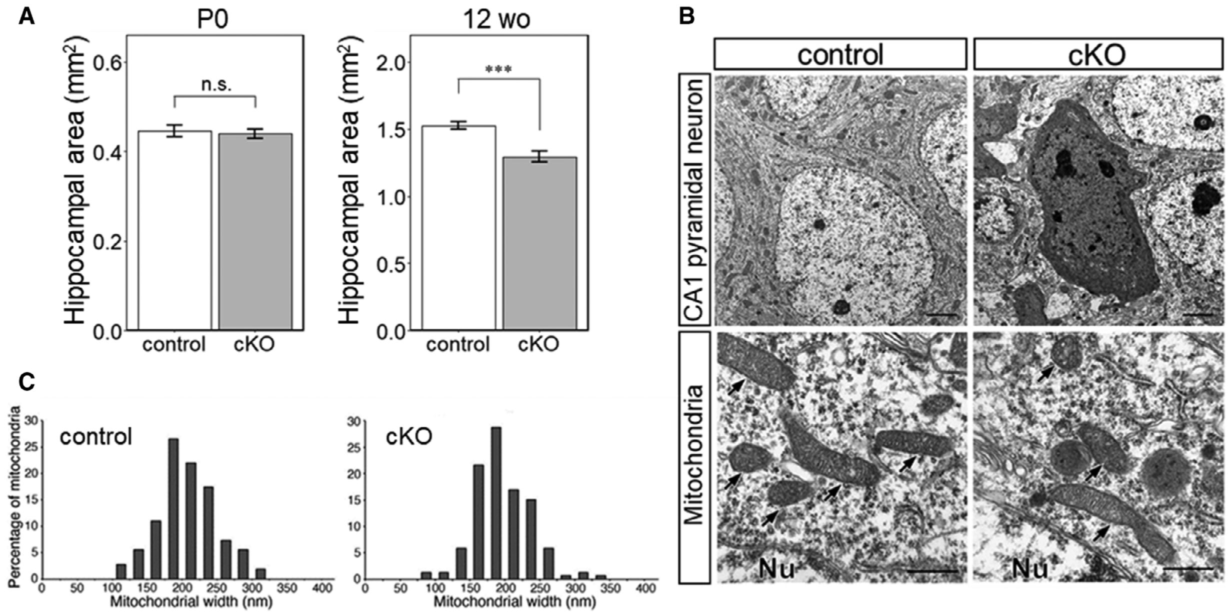

Fig. 3. *Alkbh1* deletion induced hippocampal atrophy and abnormal CA1 pyramidal neurons. (A) Quantification of the hippocampal areas of the control and *Alkbh1* cKO mice at P0 and 12 weeks of age (12 wo). We analyzed the slices at distances between 450 and 550 μm from the midline in P0 mice. The slices were obtained at distances between 480 and 600 μm from the midline at 12 weeks of age. $n = 12$ slices from 3 mice of each genotype at P0, and $n = 6$ slices from 3 mice of each genotype at 12 weeks of age. Values are means ± SEM. ***$p < 0.001$, Student's *t*-test. n.s., not significant. (B) Representative electron microscopic images of the CA1 pyramidal neurons of the control and *Alkbh1* cKO hippocampi at 27 weeks of age. High magnitude images of mitochondria in CA1 pyramidal neurons are shown in lower panels. Arrows indicate mitochondria. Nu indicates nucleus. Scale bars, 2 μm (upper two panels) and 500 nm (lower two panels). (C) Histograms of the distribution of mitochondrial width of control and *Alkbh1* cKO CA1 pyramidal neurons.

S1 and S2), suggesting that the hippocampus of *Alkbh1* cKO mice was atrophied with age. Examination of the CA1 pyramidal neurons and mitochondrial morphology of 27-week-old mice by electron microscopy (Fig. 3B) showed apparently normal mitochondrial morphology (Fig. 3B, lower panels). Furthermore, quantitative analysis of mitochondrial morphology revealed no abnormalities in mitochondrial width (Fig. 3C). However, we occasionally observed neurons with electron-dense cytoplasm and nucleoplasm in the hippocampal pyramidal cell layer (Fig 3B, upper panels). Although these dark neurons have intact membrane organelles without apparent apoptotic appearance, such as pyknotic nuclei, we did not observe such dark neurons in the control samples, suggesting that these cells may have been in the early phase of degeneration.

Alkbh1 cKO mice showed impaired hippocampus-dependent learning and memory

Loss of ALKBH1 leads to the inhibition of f^5C formation, which is also caused by pathogenic point mutations in the mt-tRNA^{Met} gene. Patients with these mutations have been implicated in autism spectrum disorder and intellectual disability [4,24,25]. Moreover, the observations of hippocampal atrophy and pyramidal cell abnormalities obtained from the histological analysis of *Alkbh1* cKO mice suggest dysfunction of hippocampus-dependent learning in these mice. Thus, we performed two types of behavioral tests evaluating hippocampus-dependent learning and memory. Because the discovered hippocampal atrophy was associated with aging, older mice (40–46 weeks of age) were used in these tests.

Firstly, we performed a contextual-dependent and auditory cued-dependent fear-conditioning test. We observed a significant decrease in hippocampus-dependent contextual memory in cKO mice, but no significant difference in hippocampal and amygdala-related cued memory retrieval (Fig. 4A). Secondly, we conducted the Morris water maze tests. Following spatial learning sessions for 5 consecutive days, the *Alkbh1* cKO mice showed significantly longer escape latency on day 5 (Fig. 4B). Twenty-four hours after the last learning session trial (day 5), the platform was removed, and all mice were given one 60-s probe trial for searching (probe test). The *Alkbh1* cKO mice spent less time in the target quadrant than the controls (Fig. 4C). These results indicated impaired

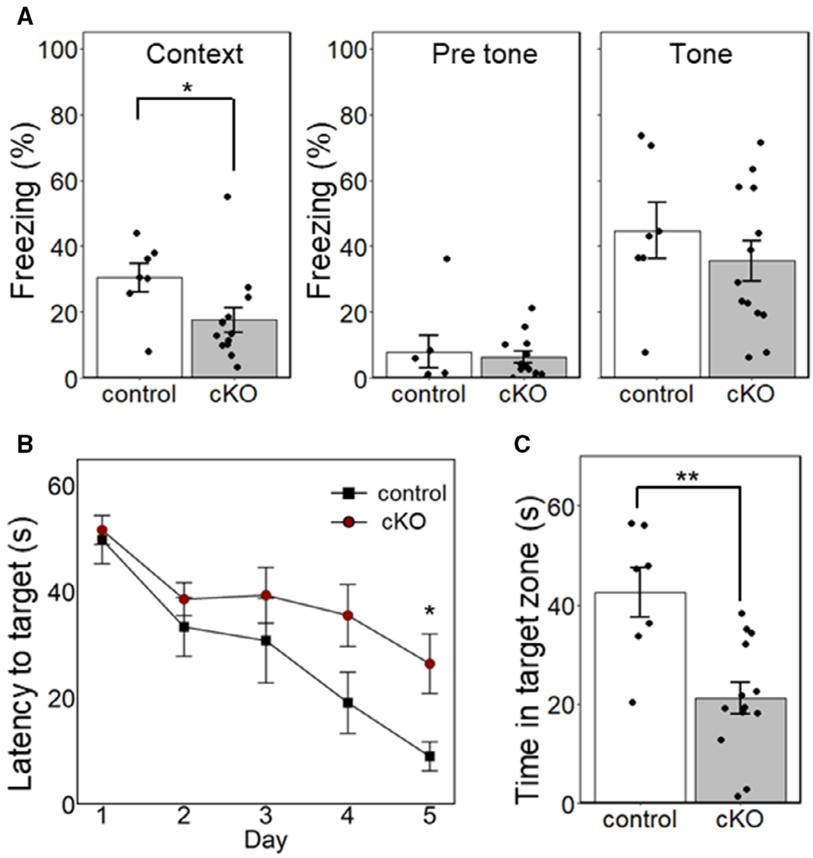

Fig. 4. *Alkbh1* cKO mice showed impaired hippocampus-dependent learning and memory. (A) Fear-conditioning test (control, $n = 7$; cKO, $n = 13$. 45–46 weeks of age). The percentage of context-dependent freezing (left graph) and cue-dependent freezing (right two graphs). The hippocampus-dependent contextual memory was significantly reduced in cKO mice. (B, C) Morris water maze test (control, $n = 7$; cKO, $n = 13$. 40 weeks of age) (B) The time taken to reach the platform in spatial learning sessions. (C) The time spent in target quadrant in probe test. Values are means ± SEM. $*p < 0.05$, $**p < 0.01$, Student's *t*-test. The time taken to reach the platform on day 5 of spatial learning was significantly longer in cKO mice, and in the probe test, cKO mice stayed in the target quadrant for less time than control.

hippocampus-dependent spatial memory in the *Alkbh1* cKO mice, a behavioral abnormality that may be associated with hippocampal atrophy.

Discussion

We and others previously identified ALKBH1, an Fe^{2+}/2-OG-dependent dioxygenase, as the enzyme responsible for f^5C formation in mt-$tRNA^{Met}$ [5]. Cultured human cells lacking *ALKBH1* exhibited a remarkable decrease in mitochondrial protein synthesis and respiratory activity, indicating that ALKBH1 is essential for normal mitochondrial function [5].

In this study, we demonstrated the dorsal telencephalon-specific *Alkbh1* cKO mice showed age-related hippocampal atrophy, which led to impaired hippocampus-dependent learning and memory. The ATP supply from synaptic mitochondria at presynaptic terminals and postsynaptic spines plays a critical role in information transmission through synapses [26]. For instance, mice lacking dynamin-related protein 1, a key factor in mitochondrial morphogenesis, have impaired hippocampus-dependent spatial memory due to defective ATP supply to the synaptic terminals [27]. Considering the reduced complex I activity in the hippocampus of *Alkbh1* cKO mice, lower ATP production due to impaired oxidative phosphorylation activities could be occurring in the *Alkbh1* cKO mice brain. Reduction in ATP available for synapses is likely to cause abnormalities in hippocampal synaptic transmission, leading to deficits in hippocampus-dependent learning.

Our *Alkbh1* cKO mice showed a marked decrease in the activity of mitochondrial respiratory chain complex I in the hippocampus, and it is highly likely that the histological and behavioral abnormalities in cKO mice are derived from mitochondrial dysfunction. However, as discussed above, ALKBH1 has been reported to have a variety of functions not limited to the mitochondria. It is also possible that these phenotypes are not solely due to a failure to form the f^5C modification in mt-$tRNA^{Met}$. Considering that respiratory chain complex I is composed of both mitochondrial and nuclear genome-encoded proteins, it is quite plausible that altered expression of nuclear genome-encoded genes due to ALKBH1 loss is combined with the effects of f^5C deficiency, leading to the phenotype. Moreover, abnormalities other than the mitochondrial respiratory chain complex may also link to hippocampal defects. In order to determine which function of ALKBH1 is responsible for the phenotype, we need to generate mitochondrial or nuclear/cytoplasmic-specific knockout mice and conduct rescue experiments using mitochondria-targeted ALKBH1. Nevertheless, the observation that hippocampal dysfunction occurred in dorsal telencephalon-specific *Alkbh1* cKO mice is an important finding and a first step toward understanding the whole picture of a multifunctional enzyme-like ALKBH1.

Spatial memory impairment has been observed in several neuropsychological disorders. Pathogenic mutations (A4435G and C4437 U) in mt-tRNA^{Met}, which inhibit f^5C formation [4], cause autism spectrum disorder and intellectual disability [24,25]. The hippocampus-dependent learning deficit observed in *Alkbh1* cKO mice might replicate the neuropsychological deficits in these patients.

The biogenesis of f^5C is mediated by two enzymes, NOL1/NOP2/Sun domain-containing protein 3 (NSUN3) and ALKBH1 [4,5]. Thus, f^5C formation is disturbed by mutations in either *ALKBH1* or *NSUN3*. Patients with *NSUN3* mutations show a combined developmental disability and microcephaly [28,29]. These symptoms were not completely consistent with the phenotype observed in our established *Alkbh1* KO mice. Given that ALKBH1 is a multifunctional enzyme, the phenotypic inconsistency between *NSUN3* deletion patients and *Alkbh1* KO mice could be due to ALKBH1 functions other than f^5C formation.

To date, two lines of *Alkbh1* KO mice have been generated and analyzed [20,22,30]. Pan *et al.* generated *Alkbh1*$^{-/-}$ mice using 129 Sv/Ev embryonic stem cells and reported that these mice showed defects in placental trophoblast lineage differentiation [30]. However, they observed no reduction in viability. The genetic backgrounds of their mice were not described other than 129 Sv/Ev. In contrast, Nordstrand *et al.* generated *Alkbh1*$^{-/-}$ mice with a hybrid genetic background between 129SvJ and C57BL/6 mice, which showed severely reduced birth rates and developmental abnormalities in the eyes and neural tube [20,22]. Here, we generated *Alkbh1* KO mice in pure C57BL/6N genetic background and analyzed their phenotypes. Our *Alkbh1* KO mice showed severe decline in both survival and body weight, consistent with the phenotype of the latter reported strain.

There are several possible explanations for the phenotypic discrepancy among the *Alkbh1* KO mouse strains. First, it is generally assumed that mice of the hybrid strains exhibit unstable phenotypes due to background effects in mutagenesis [31]. The phenotypic discordance in *Alkbh1* KO mice strains reported in previous studies may be attributed to differences in genetic backgrounds. Because our *Alkbh1* KO and cKO mice had pure C57BL/6N genetic backgrounds, we believe that our mice should be standard mouse lines to elucidate the physiological roles of Alkbh1 *in vivo*. Another possibility is the off-target effects of sgRNAs [32]. Although we used CRISPRdirect (https://crispr.dbcls.jp/) to design sgRNAs with as few off-targets as possible, it is difficult to completely exclude the possibility of off-targets. Thus, off-target mutations by sgRNAs also might contribute to the phenotypic discrepancies in the whole-body KO mice. On the other hand, in our study with cKO mice, we used *Alkbh1*-flox mice as controls, which should carry the same off-target mutations as cKO mice. Therefore, phenotypic differences between cKO and control mice can be attributed only to the deletion of Alkbh1.

In summary, the whole-body *Alkbh1* KO mice showed decreased survival and body weight, suggesting that ALKBH1 is indispensable for proper perinatal development. Furthermore, telencephalon-specific *Alkbh1* cKO mice displayed age-related hippocampal atrophy and CA1 pyramidal neuron abnormalities. Fear-conditioning and Morris water maze tests showed hippocampus-dependent learning and memory deficits in the cKO mice. These findings suggest the pivotal roles of ALKBH1 in the hippocampal neurons, emphasizing that ALKBH1 activity is essential for hippocampal function.

In conclusion, this study using our *Alkbh1* cKO mice shed light on the novel roles of ALKBH1 in the central nervous system.

Acknowledgements

We would like to thank Ryoko Kudo, Motoki Goto, Moe Tamano, and Daisuke Tanaka for generation of *Alkbh1* KO and cKO mice and all laboratory members for their support in this work. We are also grateful to Tsutomu Suzuki and Takeo Suzuki for their constructive discussions and continuous support. This work was supported by JSPS KAKENHI (18J22295 to L.K.).

Author contributions

LK and AA conceived and designed the study. LK mainly performed experiments. MF contributed to the electron microscopy analysis. RS and HK performed histological experiments. HS and AA supervised the study. LK and AA wrote the manuscripts and all authors made manuscript revisions.

Data accessibility

The data that support the findings of this study are available from the corresponding author [aiba@m.u-tokyo.ac.jp] upon reasonable request.

References

1 Suzuki T and Nagao A (2011) Human mitochondrial tRNAs: biogenesis, function, structural aspects, and diseases. *Annu Rev Genet* **45**, 299–329. https://doi.org/10.1146/annurev-genet-110410-132531

2 Moriya J, Yokogawa T, Wakita K, Ueda T, Nishikawa K, Crain PF, Hashizume T, Pomerantz SC and McCloskey JA (1994) A novel modified nucleoside found at the first position of the anticodon of methionine tRNA from bovine liver-mitochondria. *Biochemistry* **33**, 2234–2239. https://doi.org/10.1021/bi00174a033

3 Takemoto C, Spremulli LL, Benkowski LA, Ueda T, Yokogawa T and Watanabe K (2009) Unconventional decoding of the AUA codon as methionine by mitochondrial $tRNA^{Met}$ with the anticodon f^5CAU as revealed with a mitochondrial in vitro translation system. *Nucleic Acids Res* **37**, 1616–1627. https://doi.org/10.1093/nar/gkp001

4 Nakano S, Suzuki T, Kawarada L, Iwata H, Asano K and Suzuki T (2016) NSUN3 methylase initiates 5-formylcytidine biogenesis in human mitochondrial $tRNA^{Met}$. *Nat Chem Biol* **12**, 546–551. https://doi.org/10.1038/nchembio.2099

5 Kawarada L, Suzuki T, Ohira T, Hirata S and Miyauchi K (2017) ALKBH1 is an RNA dioxygenase responsible for cytoplasmic and mitochondrial tRNA modifications. *Nucleic Acids Res* **45**, 7401–7415. https://doi.org/10.1093/nar/gkx354

6 Haag S, Sloan KE, Ranjan N, Warda AS, Kretschmer J, Blessing C, Hübner B, Seikowski J, Dennerlein S, Rehling P *et al.* (2016) NSUN3 and ABH1 modify the wobble position of mt-$tRNA^{Met}$ to expand codon recognition in mitochondrial translation. *EMBO J* **35**, 2104–2119. https://doi.org/10.15252/embj.201694885

7 Liu FG, Clark W, Luo GZ, Wang XY, Fu Y, Wei JB, Wang X, Hao Z, Dai Q, Zheng G *et al.* (2016) ALKBH1-mediated tRNA demethylation regulates translation. *Cell* **167**, 816–828. https://doi.org/10.1016/j.cell.2016.09.038

8 Rashad S, Han X, Sato K, Mishima E, Abe T, Tominaga T and Niizuma K (2020) The stress specific impact of ALKBH1 on tRNA cleavage and tiRNA generation. *RNA Biol* **17**, 1092–1103. https://doi.org/10.1080/15476286.2020.1779492

9 Wu TP, Wang T, Seetin MG, Lai YQ, Zhu SJ, Lin KX, Liu Y, Byrum SD, Mackintosh SG, Zhong M *et al.* (2016) DNA methylation on N-6-adenine in mammalian embryonic stem cells. *Nature* **532**, 329–333. https://doi.org/10.1038/nature17640

10 Xie Q, Wu TP, Gimple RC, Li Z, Prager BC, Wu Q, Yu Y, Wang P, Wang Y, Gorkin DU *et al.* (2018) N6-methyladenine DNA Modification in Glioblastoma. *Cell* **175**, 1228–1243.e20. https://doi.org/10.1016/j.cell.2018.10.006

11 Li H, Zhang Y, Guo Y, Liu R, Yu Q, Gong L, Liu Z, Xie W and Wang C (2020) ALKBH1 promotes lung cancer by regulating m6A RNA demethylation. *Biochem Pharmacol* 114284. https://doi.org/10.1016/j.bcp.2020.114284

12 Zorov DB, Juhaszova M and Sollott SJ (2014) Mitochondrial reactive oxygen species (ROS) and ROS-induced ROS release. *Physiol Rev* **94**, 909–950. https://doi.org/10.1152/physrev.00026.2013

13 Mattiasson G, Friberg H, Hansson M, Elmer E and Wieloch T (2003) Flow cytometric analysis of mitochondria from CA1 and CA3 regions of rat hippocampus reveals differences in permeability transition pore activation. *J Neurochem* **87**, 532–544. https://doi.org/10.1046/j.1471-4159.2003.02026.x

14 Swerdlow RH (2018) Mitochondria and mitochondrial cascades in Alzheimer's disease. *J Alzheimers Dis* **62**, 1403–1416. https://doi.org/10.3233/jad-170585

15 Gurumurthy CB, O'Brien AR, Quadros RM, Adams J, Alcaide P, Ayabe S, Ballard J, Batra SK, Beauchamp MC, Becker KA *et al.* (2019) Reproducibility of CRISPR-Cas9 methods for generation of conditional mouse alleles: a multi-center evaluation. *Genome Biol* **20**, 171. https://doi.org/10.1186/s13059-019-1776-2

16 Kassai H, Terashima T, Fukaya M, Nakao K, Sakahara M, Watanabe M and Aiba A (2008) Rac1 in cortical projection neurons is selectively required for midline crossing of commissural axonal formation. *Eur J Neurosci* **28**, 257–267. https://doi.org/10.1111/j.1460-9568.2008.06343.x

17 Trounce IA, Kim YL, Jun AS and Wallace DC (1996) Assessment of mitochondrial oxidative phosphorylation in patient muscle biopsies, lymphoblasts, and transmitochondrial cell lines. *Methods Enzymol* **264**, 484–509. https://doi.org/10.1016/s0076-6879(96)64044-0

18 Saito R, Koebis M, Nagai T, Shimizu K, Liao J, Wulaer B, Sugaya Y, Nagahama K, Uesaka N, Kushima I *et al.* (2020) Comprehensive analysis of a novel mouse model of the 22q11.2 deletion syndrome: a model with the most common 3.0-Mb deletion at the human 22q11.2 locus. *Transl Psychiatry* **10**, 35. https://doi.org/10.1038/s41398-020-0723-z

19 Tian LF, Liu YP, Chen LQ, Tang Q, Wu W, Sun W, Chen Z and Yan XX (2020) Structural basis of nucleic acid recognition and 6mA demethylation by human ALKBH1. *Cell Res* **30**, 272–275. https://doi.org/10.1038/s41422-019-0233-9

20 Nordstrand LM, Svard J, Larsen E, Nilsen A, Ougland R, Furu K, Lien GF, Rognes T, Namekawa SH, Lee JT *et al.* (2010) Mice lacking Alkbh1 display sex-ratio distortion and unilateral eye defects. *PLoS ONE* **5** (11), e13827. https://doi.org/10.1371/journal.pone.0013827

21 Iwasato T, Datwani A, Wolf AM, Nishiyama H, Taguchi Y, Tonegawa S, Knöpfel T, Erzurumlu RS and Itohara S (2000) Cortex-restricted disruption of NMDAR1 impairs neuronal patterns in the barrel cortex. *Nature* **406**, 726–731. https://doi.org/10.1038/35021059

22 Ougland R, Lando D, Jonson I, Dahl JA, Moen MN, Nordstrand LM, Rognes T, Lee JT, Klungland A, Kouzarides T*et al.* (2012) ALKBH1 Is a Histone H2A Dioxygenase Involved in Neural Differentiation. *Stem Cells* **30**, 2672–2682. https://doi.org/10.1002/stem.1228

23 Wang XK and Michaelis EK (2010) Selective neuronal vulnerability to oxidative stress in the brain. *Front Aging Neurosci* **2**, 12. https://doi.org/10.3389/fnagi.2010.00012

24 Valiente-Palleja A, Torrell H, Muntane G, Cortes MJ, Martinez-Leal R, Abasolo N, Vilella E and Martorell L (2018) Genetic and clinical evidence of mitochondrial dysfunction in autism spectrum disorder and intellectual disability. *Hum Mol Genet* **27**, 891–900. https://doi.org/10.1093/hmg/ddy009

25 Wang YQ, Picard M and Gu ZL. (2016) Genetic evidence for elevated pathogenicity of mitochondrial DNA heteroplasmy in autism spectrum disorder. *PLOS Genet* **12**, e1006391. https://doi.org/10.1371/journal.pgen.1006391

26 Harris JJ, Jolivet R and Attwell D (2012) Synaptic energy use and supply. *Neuron* **75**, 762–777. https://doi.org/10.1016/j.neuron.2012.08.019

27 Oettinghaus B, Schulz JM, Restelli LM, Licci M, Savoia C, Schmidt A, Schmitt K, Grimm A, Morè L, Hench J *et al.* (2016) Synaptic dysfunction, memory deficits and hippocampal atrophy due to ablation of mitochondrial fission in adult forebrain neurons. *Cell Death Differ* **23**, 18–28. https://doi.org/10.1038/cdd.2015.39

28 Van Haute L, Dietmann S, Kremer L, Hussain S, Pearce SF, Powell CA, Rorbach J, Lantaff R, Blanco S, Sauer S *et al.* (2016) Deficient methylation and formylation of mt-tRNAMet wobble cytosine in a patient carrying mutations in NSUN3. *Nat Commun* **7**, 12039. https://doi.org/10.1038/ncomms12039

29 Paramasivam A, Meena AK, Venkatapathi C, Pitceathly RDS and Thangaraj K. (2020) Novel Biallelic NSUN3 Variants Cause Early-Onset Mitochondrial Encephalomyopathy and Seizures. *J Mol Neurosci* **70**, 1962–1965. https://doi.org/10.1007/s12031-020-01595-8

30 Pan ZS, Sikandar S, Witherspoon M, Dizon D, Nguyen T, Benirschke K, Wiley C, Vrana P and Lipkin SM (2008) Impaired placental trophoblast lineage differentiation in *Alkbh1*$^{-/-}$ mice. *Dev Dyn* **237**, 316–327. https://doi.org/10.1002/dvdy.21418

31 Sittig LJ, Carbonetto P, Engel KA, Krauss KS, Barrios-Camacho CM and Palmer AA (2016) Genetic background limits generalizability of genotype-phenotype relationships. *Neuron* **91**, 1253–1259. https://doi.org/10.1016/j.neuron.2016.08.013

32 Tuladhar R, Yeu Y, Piazza JT, Tan Z, Clemenceau JR, Wu XF, Barrett Q, Herbert J, Mathews DH, Kim J *et al.* (2019) CRISPR-Cas9-based mutagenesis frequently provokes on-target mRNA misregulation. *Nat Commun* **10**, 4056. https://doi.org/10.1038/s41467-019-12028-5

Supporting information

Additional supporting information may be found online in the Supporting Information section at the end of the article.

Figure S1 Nissl-stained sagittal sections of the hippocampus in the control (top 12 panels) and Alkbh1cKO(bottom 12 panels) mice at P0.

Figure S2 Nissl-stained sagittal sections of the hippocampus in the control (top 6 panels) and Alkbh1cKO(bottom 6 panels) mice at 12 weeks of age.